Daniel Peterseim

Numerical Homogenization of Partial Differential Equations

Lecture notes for participants of the

Winter School on Numerical Analysis of Multiscale Problems,

Hausdorff Insitut of Mathematics Bonn, January 9-13, 2017.

Preliminary version of 11th January 2017.

Preface

The objective of these lecture notes is to introduce quickly the reader to numerical homogenization. The choice of the material is rather personal and strongly influenced by our own work in this context. The manuscript is not not meant to to give a complete overview of numerical homogenization and its mathematical background but to make the reader familiar with the underlying ideas of two central approaches in this context.

These notes where written during courses held at the University of Bonn in 2014 and 2016. I would like to thank Denis Dsseldorf, Dietmar Gallistl, Roland Maier and Mira Schedensack for their help in producing and proof-reading earlier drafts. The manuscript is still under construction and has a preliminary character and some parts need some improvement and completion.

Bonn, January 2017 *Daniel Peterseim*

Contents

Chapter 1
Introduction

Abstract Many physical processes in microheterogeneous media such as modern composite and functional materials are described by partial differential equations (PDEs) with rough coefficients or domains with a complex microstructure. This chapter presents a few examples. Given the complexity of these processes, the key to reliably simulate some relevant classes of such processes involves the construction of appropriate macroscopic (homogenized or effective) models. This is illustrated by studying a one-dimensional model problem of oscillatory diffusion.

1.1 Multiscale Problems

Heterogeneous micro-structures on many non-separable scales and high contrast in physical properties of the constituents are key features for the superior behaviour of modern composite and multi-functional materials. However, these features cause major difficulties for their computer simulation. The resolution of all characteristic length scales is prohibitively expensive while the naive disregard of relevant microscopic information leads to questionable results, even on macroscopic scales of interest.

Homogenization methods try to remedy this dilemma. They account for the relevant microscopic information in a hierarchical, concurrent and adaptive fashion so that a reliable simulation of multiscale problems eventually becomes feasible in state-of-the-art computing environments. This lecture concerns the design of the related numerical algorithms and, equally important, the mathematics behind them to foresee and assess their reliability and efficiency in engineering and scientific applications.

Among the target applications of this lecture is the mechanical analysis of multiphase materials such as composite and multifunctional materials. The manipulation of characteristics and relative volumes of its constituents allows one to equip engineered multiphase materials with some targeted portfolio of physical properties (e.g. light-weight, stiffness, strong electric and magnetic order, energy conver-

sion). The development of novel multifunctional materials for the next-generation of performance-tailored structures requires the topological optimisation of the microstructures and, hence, the understanding how certain material properties (conductivity, permeability, etc.) depend on controllable variables (thermal conductivities of the constituents, relative volumes, particles shapes, coating and size).

Transport processes in porous media, e.g. groundwater flow in unsaturated soils [16, 18], share the previous challenges in that the occurring permeabilities and hydraulic conductivities have rapidly changing features due to different types of soil, microscopic inclusions in the bottom or porous subsurface rock formations. Any meaningful numerical simulation of relevant physical effects has to account for these highly heterogeneous fine scale structures in the whole computational domain. If pore scale effects become relevant or if domains spread over kilometers, the computational load easily exceeds computer capacity when standard finite element or finite volume methods are used.

1.2 Modeling diffusion in heterogeneous media

We shall briefly recall some elementary ingredients of the mathematical modeling of diffusion. Imagine a *motionless* medium filling a straight (thin) tube and a substance that is diffusing through it. Given the concentration u of the substance at time $t = 0$, we are aiming for an equation that describes the concentration of the substance at later times. The amount of substance that passes the point x from left to right per unit time is called *flux* $q(x,t)$. If the substance flows from right to left, then the flux is negative. We are assuming conservation of mass, i.e., for any control volume (x_0, x_1), the mass

$$M = \int_{x_0}^{x_1} u(x,t)\,dx$$

changes in time by in- or outflow only, i.e.,

$$\frac{d}{dt}M = q(x_0,t) - q(x_1,t).$$

In short, what flows in (at x_0) and never flows out (at x_1), increases the mass M. Hence,

$$\int_{x_0}^{x_1} u_t(x,t)dx = q(x_0,t) - q(x_1,t)$$

and, after differentiation with respect to x_1 and the replacement $x_1 \to x$,

$$\frac{d}{dt}u = -\frac{d}{dx}q \quad \text{in } Q = (0,1)\times[0,T].$$

This conservation law does not suffice to determine u and q. We rather need a second hypothesis that connects the concentration and the flux -- a diffusion law. While the mass balance features a direct plausibility (*first principle*), the diffusion law is the

result of experimental and phenomenological studies. The simplest diffusion law (Fick's first law) says that the flux depends linearly on u_x, i.e.

$$q(x,t) = -A(x)\frac{d}{dx}u(x,t).$$

The diffusivity $A(x) > 0$ is a characteristic property of the material at the point x and has to be measured. In homogeneous media, A may be treated as a global constant. In heterogeneous media, A varies with spatial location. E.g., the coefficient A takes two different values in the constituents of the composite.

Finally, we model the process of diffusion by the linear differential equation

$$\frac{d}{dt}u = (Au_x)_x \quad \text{in } Q = (0,1)\times[0,T] \tag{1.1}$$

along with the initial condition

$$u(x,0) = u_0(x) \quad (0 \le x \le 1),$$

where u_0 denotes the known concentration at time $t = 0$. If we want to model that no substance can enter or escape at the ends of the tube, then by Fick's law the concentration gradient has to vanish there, i.e.,

$$\frac{d}{dx}u(0,t) = \frac{d}{dx}u(1,t) = 0 \quad (0 \le t \le T). \tag{1.2}$$

These boundary conditions are called *Neumann boundary conditions*.

Equation (1.1) also models heat conduction in a thin wire and is therefore also known as the *heat equation*. The boundary conditions (1.2) then model that the wire is perfectly insulated at its ends. If instead the temperature is prescribed at the ends, we employ boundary conditions

$$u(0,t) = g_0(t), \quad u(1,t) = g_1(t) \quad (0 \le t \le T) \tag{1.3}$$

with given functions g_0 and g_1. These boundary conditions are called *Dirichlet boundary conditions*.

Often, we are interested in the steady state solution of the system, i.e., the equilibrium concentration after long time if data remains unchanged, i.e., $\frac{d}{dt}u = 0$. This yields the stationary heat equation

$$-\frac{d}{dx}\left(A(x)\frac{d}{dx}u(x)\right) = 0 \quad \text{in} \quad D = (0,1) \tag{1.4}$$

with Dirichlet boundary condition

$$u(0) = g_0, \quad u(1) = g_1 \tag{1.5}$$

for some given (time-invariant) boundary values g_0 and g_1. For a constant diffusivity (or thermal conductivity) A, this equation is known as the Laplace equation and its solutions are called harmonic functions.

In the presence of further forces such as gravity or external heat sources in a multi-dimensional setting, we end up with the Poisson-type model problem

$$-\operatorname{div} A(x)\nabla u(x) = f(x) \quad \text{in } D \subset \mathbb{R}^d \tag{1.6}$$

with Dirichlet boundary conditions

$$u(x) = g(x) \quad \text{for } x \in \partial D. \tag{1.7}$$

In anisotropic materials, the thermal conductivity typically varies with orientation; in this case A is represented by a positive definite matrix ($A : D \to \mathbb{R}^{d\times d}$).

The problem (1.6)--(1.7) will serve as a prototypical example for which we will study several discretization schemes. It is an important building block of more general multi-physics problems, e.g. in the context of geophysical flows through porous media. Given the permeability κ of the rock, the total mobility $\mu(s)$, the fractional flow f, and sink and source terms g, q, the task is to find the pressure p and the water concentration s such that

$$-\operatorname{div}(\mu(s)\kappa\nabla p) = q, \quad \frac{d}{dt}s - \operatorname{div}(f(s)\mu(s)\kappa\nabla p) = g \quad \text{in } D.$$

Since κ is stationary and $\mu(s)$ only changes at the water front, an elliptic problem with some rough diffusion tensor $k = \kappa\mu(s)$ needs to be solved in each time step. Recall that κ varies on the scale of pores in the rock whereas we are interested in simulating the flow over meters and kilometers. For further details regarding this particular application, we refer to [9, Chapter 1].

1.3 Highly oscillatory diffusion in one dimension

For the illustration of the critical scaling effects that motivate this lecture, we shall consider the simplest possible model problem, that is, a one-dimensional diffusion problem in a periodic laminate,

$$\left.\begin{aligned} -\frac{d}{dx}\left(A_\varepsilon(x)\frac{d}{dx}u_\varepsilon(x)\right) = f(x) \quad \text{in } (0,1), \\ u_\varepsilon(0) = u_\varepsilon(1) = 0, \end{aligned}\right\} \tag{1.8}$$

with some smooth forcing term f and a uniformly positive, smooth, periodic diffusion coefficient A_ε with some small parameter $\varepsilon > 0$ that reflects the period length. The problem admits a unique solution u_ε in the Sobolev space $H^1_0(0,1)$ that is as well characterized by the variational formulation

$$\int_0^1 A_\varepsilon u_\varepsilon' v' \, dx = \int_0^1 f v \, dx \quad \text{for all } v \in H_0^1(0,1). \tag{1.9}$$

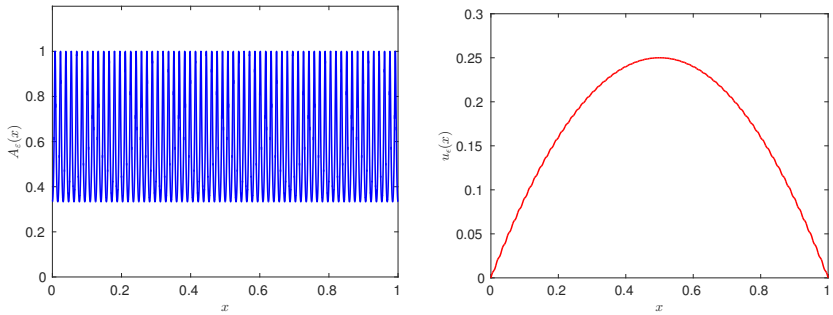

(a) Highly oscillatory diffusivity defined in (1.10) for $\varepsilon = 2^{-6}$.

(b) Corresponding solution u_ε of (1.9) for $\varepsilon = 2^{-6}$.

Fig. 1.1 Illustration of model problem (1.8) for $\varepsilon = 2^{-6}$.

1.3.1 Naive finite element discretization and pre-asymptotic effects

We shall study the particular instance of problem (1.9) with data $f \equiv 1$ and A_ε given by

$$A_\varepsilon(x) := \left(2 + \cos\left(2\pi \frac{x}{\varepsilon}\right)\right)^{-1} \tag{1.10}$$

for some small parameter $\varepsilon > 0$ such that $\varepsilon^{-1} \in \mathbb{N}$; cf. Figure 1.1a. In this one-dimensional setting, the corresponding unique solution

$$u_\varepsilon = x - x^2 + \varepsilon\left(\tfrac{1}{4\pi}\sin(2\pi\tfrac{x}{\varepsilon}) - \tfrac{1}{2\pi} x \sin(2\pi\tfrac{x}{\varepsilon}) - \tfrac{\varepsilon}{4\pi^2}\cos(2\pi\tfrac{x}{\varepsilon}) + \tfrac{\varepsilon}{4\pi^2}\right) \tag{1.11}$$

of (1.8) is easily computed and allows us to study the performance of numerical techniques.

The numerical solution of second order elliptic partial differential equations and beyond is very well established. Nowadays the most popular scheme is the Galerkin finite element method. For symmetric problems such as our model problem, the Galerkin method seeks the best approximation $u_{\varepsilon,h}$ of u_ε (with respect to the scalar product on the right-hand side of (1.9)) within some finite-dimensional subspace $V_h \subset H_0^1(0,1)$. Among the most popular choices of subspace are conforming first-order finite elements (P_1-FEM) on a uniform grid

$$\mathcal{T}_h := \{[jh, (j+1)h] \,|\, j = 0, \ldots, 1/h\}$$

of the unit interval with mesh-size parameter $0 < h < 1$ (such that $h^{-1} \in \mathbb{N}$). In this case, the approximation space reads

$$V_h = \{w \in C^0(0,1) \mid \forall T \in \mathcal{T}_h,\ w|_T \text{ is affine and } w(0) = w(1) = 0\} \tag{1.12}$$

and the finite element approximation $u_{\varepsilon,h} \in V_h$ is uniquely characterized by the discrete variational problem

$$\int_0^1 A_\varepsilon u'_{\varepsilon,h} v'_h \, dx = \int_0^1 f v_h \, dx \quad \text{for all } v_h \in V_h. \tag{1.13}$$

By a choice of basis of V_h, this problem may be rephrased as a system of linear algebraic equations in the coefficients of the basis representation of $u_{\varepsilon,h}$.

We shall study the performance of this method for several choices of parameters -- modeling parameter ε (typically given) and the mesh size parameter h (to be chosen). The subsequent Matlab code generates the Galerkin approximations $u_{\varepsilon,h} \in V_h$ and produces some graphical output. Note that the code relies on highly accurate adaptive quadrature of the oscillatory coefficient to reproduce the (almost) exact Galerkin approximation of (1.13) and to exclude significant errors originating from numerical quadrature.

Example 1.1 (Finite element approximation of model problem (1.9)*).*

```
% script file for illustration of FEM for 1d oscillatory diffusion
clear all
close all

% define Interval
I = [0,1];

% define diffusivity
epsilon = 2^(-15);
A = @(x) 1./(2+cos(2*pi*x./epsilon));

% plot coefficient
figure(1)
t = 0:0.0001:1;
hcoeff = plot(t,A(t),'b','LineWidth',2)
hold on
set(gca,'Fontsize',18)
axis([0 1 0 1.2*max(A(t))]);
xlabel('$x$','Fontsize',18,'Interpreter','latex')
ylabel('$A_{\varepsilon}(x)$','Fontsize',18,'Interpreter','latex')
latexprint(strcat('../../LectureNotes/gfx/oscdiff1d_coeff_',...
          num2str(-log2(epsilon))),'-r600')

% forcing term
f = @(x) ones(size(x));

% solution
uepsilon = @(x) x - x.^2 ...
```

```
             + epsilon*(-1/(2*pi)*x.*sin(2*pi*x/epsilon)...
                       + 1/(4*pi)*sin(2*pi*x/epsilon)...
                       - epsilon/(4*pi^2)*cos(2*pi*x/epsilon)+...
                       + epsilon/(4*pi^2));

% plot solution
figure(2)
hsol = plot(t,uepsilon(t),'r','LineWidth',2);
hold on
set(gca,'Fontsize',18)
axis([0 1 0 1.2*max(uepsilon(t))]);
xlabel('$x$','Fontsize',18,'Interpreter','latex')
ylabel('$u_\epsilon(x)$','Fontsize',18,'Interpreter','latex')
latexprint(strcat('../../LectureNotes/gfx/oscdiff1d_sol_',...
          num2str(-log2(epsilon))),'-r600')

% finite element approximation on equi-distant grid
for k=1:15
   % finte element grid
   N = 1+2^k; % number of grid points
   h(k) = 1/(N-1); % mesh size
   x = (0:h(k):1)';

   % stiffness matrix
   for j=1:N-1
      Amean(j)=quadgk(@(x) A(x),x(j),x(j+1),'RelTol',1e-8)./h(k);
   end

   Ndof = N-2;
   S = sparse(1:Ndof,1:Ndof,1/h(k).*(Amean(1:N-2)+...
                                Amean(2:N-1)),Ndof,Ndof);
   S = S+sparse(2:Ndof,1:Ndof-1,-1/h(k).*Amean(2:N-2),Ndof,Ndof);
   S = S+sparse(1:Ndof-1,2:Ndof,-1/h(k).*Amean(2:N-2),Ndof,Ndof);

   % right hand side
   rhs = h(k)*f(x(2:N-1));

   % solve
   uk = S\rhs;
   uk = [0;uk;0]; % extend to boundary

   % plot approximation on current mesh
   figure(2)
   hfem(k) = plot(x,uk,'b','LineWidth',1);
   latexprint(strcat('../../LectureNotes/gfx/oscdiff1d_fem_',...
             num2str(k),'_',num2str(-log2(epsilon))),'-r600')

   % estimate error
   e = uepsilon(x)-uk;
   err(k) = 0;
   for j=1:N-1
      err(k) = err(k) + ...
               quadgk(@(s) (uepsilon(s)-uk(j)...
               - (uk(j+1)-uk(j))./h(k)*(s-x(j))).^2,...
```

```
            x(j),x(j+1),'RelTol',1e-8);
    end
    err(k) = sqrt(err(k));

    % plot error
    figure(3)
    herr = loglog(h,err,'-bd','LineWidth',2)
    hold on
    set(gca,'Fontsize',18,'xscale','log','yscale','log',...
        'xtick',10.^(-4:1:0),'ytick',10.^(-8:2:0))
    axis([1e-5 1 1e-10 1]);
    axis square
    grid on
    xlabel('$h$','Fontsize',18,'Interpreter','latex')
    ylabel('$\|u-u_h\|_{L^2(0,1)}$','Fontsize',18,...
          'Interpreter','latex')
    set(herr,'LineWidth',2)
    latexprint(strcat('../../LectureNotes/gfx/oscdiff1d_err_',...
              num2str(k),'_',num2str(-log2(epsilon))),'-r600')

          pause(.1)
    set(herr,'Visible','Off')
    set(hfem,'Visible','Off')
end
```

Figure 1.2 depicts the finite element approximation on different scales of numerical resolution h for fixed $\varepsilon = 2^{-6}$. The FE solutions show very different behavior in different regimes of numerical resolution. If $h \gtrsim \varepsilon$ -- the case of under-resolution -- FEM is not capable of capturing the solution, neither its microscopic oscillations nor its macroscopic behavior. The FEM solution rather seems to converge to some other function. (Guess which one!) This regime is called pre-asymptotic regime. Only if h is sufficiently small, i.e., $h \lesssim \varepsilon$, the method suddenly switches to the expected asymptotic behavior of quadratic convergence (in L^2). Figure 1.3 shows that the sharp phase transition between pre-asymptotic and the asymptotic regime is truly linked to the scale $h \approx \varepsilon$ and, hence, that the performance of FEM suffers critically from very small microstructures represented by the parameter ε. In many relevant multi-dimensional applications, the fine scales (represented by ε here) are so small that this asymptotic regime is never reached, even on large computers. The aim of this lecture is to present advanced numerical techniques to reduce such crucial scale-dependent pre-asymptotic effects in finite element and related methods.

1.3.2 Effective coefficient and periodic homogenization

Classical homogenization is a tool of mathematical modeling that seeks a simplified model that is able to capture the macroscopic responses of the problem. Note that the solution u_ε explicitly given in (1.11) is composed of some macroscopic (ε-independent) part

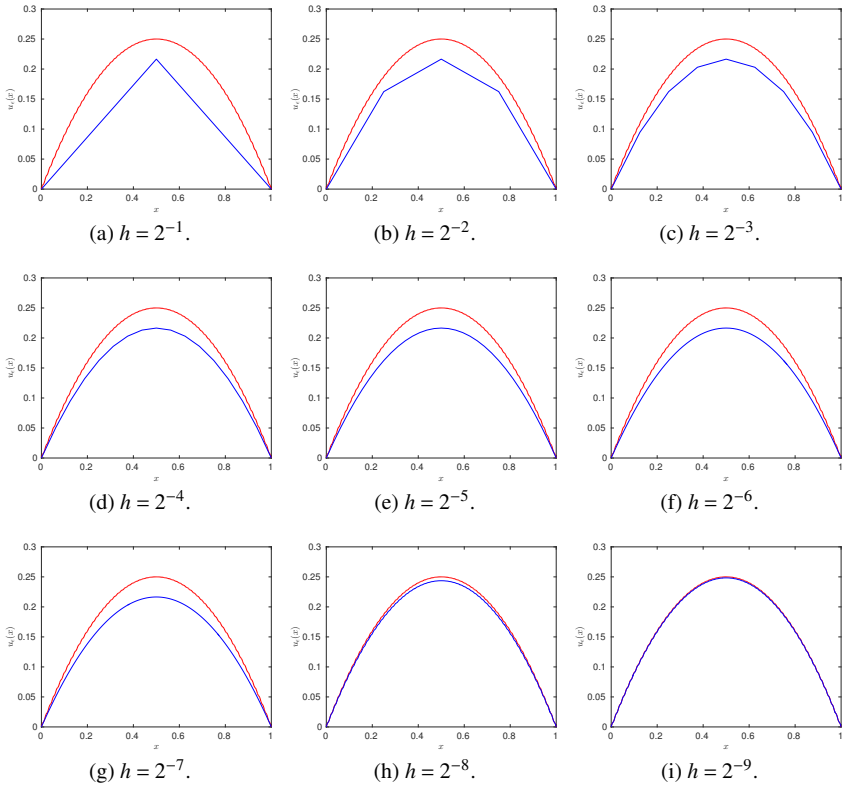

(a) $h = 2^{-1}$. (b) $h = 2^{-2}$. (c) $h = 2^{-3}$.

(d) $h = 2^{-4}$. (e) $h = 2^{-5}$. (f) $h = 2^{-6}$.

(g) $h = 2^{-7}$. (h) $h = 2^{-8}$. (i) $h = 2^{-9}$.

Fig. 1.2 Finite element approximation of model problem (1.8) for $\varepsilon = 2^{-6}$.

$$u_0 = x - x^2$$

and some microscopic (highly oscillatory and small L^2-norm) remainder

$$u_\varepsilon - u_0 = \varepsilon\left(\frac{1}{4\pi}\sin(2\pi\tfrac{x}{\varepsilon}) - \frac{1}{2\pi}x\sin(2\pi\tfrac{x}{\varepsilon}) - \frac{\varepsilon}{4\pi^2}\cos(2\pi\tfrac{x}{\varepsilon}) + \frac{\varepsilon}{4\pi^2}\right)$$

that tends to zero (in L^2) with ε. In other words,

$$u_\varepsilon \to u_0 \text{ strongly in } L^2(0,1) \text{ as } \varepsilon \to 0, \tag{1.14}$$

whereas the sequence is only bounded in $H^1(0,1)$ but not strongly convergent as oscillations get faster and faster. Moreover, one observes that u_0 is the solution of the Poisson problem

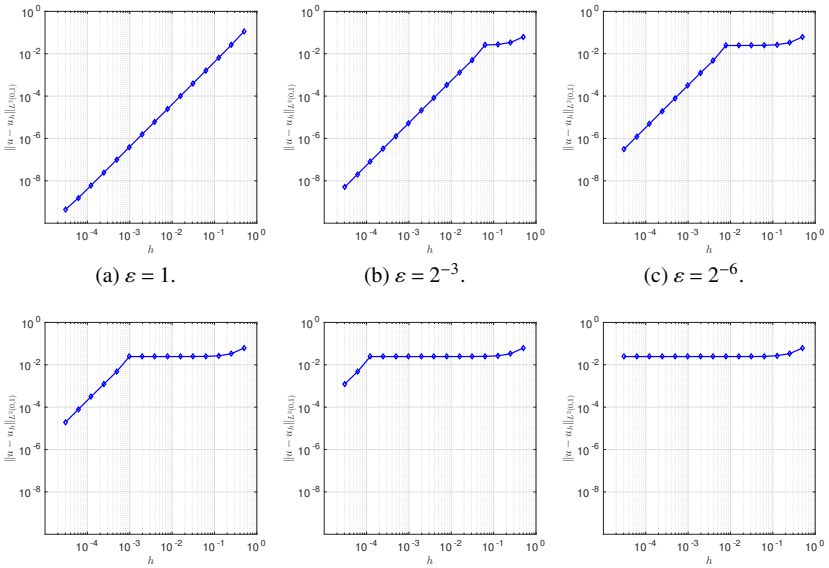

(a) $\varepsilon = 1$. (b) $\varepsilon = 2^{-3}$. (c) $\varepsilon = 2^{-6}$.

(d) $\varepsilon = 2^{-9}$. (e) $\varepsilon = 2^{-12}$. (f) $\varepsilon = 2^{-15}$.

Fig. 1.3 Finite element approximation of model problem (1.8): L^2-error vs. mesh size h for several values of the diffusion parameter ε.

$$\left.\begin{aligned} -\frac{d}{dx}\left(A_0 \frac{d}{dx} u_0(x)\right) &= f(x) \quad \text{in } (0,1), \\ u(0) = u(1) &= 0, \end{aligned}\right\} \tag{1.15}$$

with some constant $A_0 > 0$ - the so-called effective or homogenized coefficient. Is this just by coincidence for the particular $f \equiv 1$ or is there is some general mechanism behind?

Let $A_1 \in L^\infty_\#(0,1)$ be a uniformly positive, 1-periodic coefficient and define ε-periodic coefficients A_ε by $A_\varepsilon(x) := A_1(\frac{x}{\varepsilon})$. The main question of periodic homogenization then reads: Is there an effective (constant) coefficient $A_0 > 0$ such that the solutions u_ε of (1.8) converge to the solution u_0 of problem (1.15) uniformly with respect to $f \in L^2(0,1)$? If yes, Problem (1.15) is denoted homogenized (or effective) problem. (Keep in mind that, in general, the structure and the type of the homogenized problem can be very different from the structure of the original problem, it will not be the case in the present setting though.) In addition to this theoretical question, there is the equally important question of computability of the effective coefficient.

For the simple model problem of this section, both question can be answered in a positive and satisfying way in one stroke. For the time being, we assume that $A_0 > 0$ is some real number and that the tentative macroscopic part u_0 solves (1.15). We shall have a look at the L^2-error between u_ε and u_0. We restrict ourselves tacitly to values of ε that are related to integer frequencies, i.e., $\varepsilon^{-1} \in \mathbb{N}$.

Since the error $(u_\varepsilon - u_0) \in H_0^1(0,1) \subset L^2(0,1)$, there exists a unique $z \in H_0^1(0,1)$ such that

$$\int_0^1 A_0 z' w'\,dx = \int_0^1 (u_\varepsilon - u_0) w\,dx \quad \text{for all } w \in H_0^1(0,1).$$

The choice $w = u_\varepsilon - u_0$ as a test function yields that

$$\|u_\varepsilon - u_0\|_{L^2(0,1)}^2 = \int_0^1 A_0 z' (u_\varepsilon - u_0)'\,dx.$$

This relation between the L^2 error and the variational form is known as Aubin-Nitsche duality trick [2].

The solutions u_0 and u_ε are linked by the equality of fluxes

$$A_\varepsilon u_\varepsilon' = A_0 u_0' \qquad \text{in } H^{-1}(0,1),$$

that is,

$$\int_0^1 A_\varepsilon u_\varepsilon' v\,dx = \int_0^1 A_0 u_0' v\,dx \qquad \text{for all } v \in H_0^1(0,1).$$

This and some algebraic manipulations lead to

$$\begin{aligned}
\|u_\varepsilon - u_0\|_{L^2(0,1)}^2 &= \int_0^1 z'(A_0 - A_\varepsilon) u_\varepsilon'\,dx = \int_0^1 A_0 z' \frac{A_0 - A_\varepsilon}{A_0 A_\varepsilon} A_\varepsilon u_\varepsilon'\,dx \\
&= \sum_{j=1}^N \Bigg(\int_{(j-1)\varepsilon}^{j\varepsilon} \Big(A_0 z' - \varepsilon^{-1} \int_{(j-1)\varepsilon}^{j\varepsilon} A_0 z'\,dx \Big) \frac{A_0 - A_\varepsilon}{A_0 A_\varepsilon} A_\varepsilon u_\varepsilon'\,dx \\
&\quad + \varepsilon^{-1} \int_{(j-1)\varepsilon}^{j\varepsilon} A_0 z'\,dx \int_{(j-1)\varepsilon}^{j\varepsilon} \frac{A_0 - A_\varepsilon}{A_0 A_\varepsilon} \Big(A_\varepsilon u_\varepsilon' - \varepsilon^{-1} \int_{(j-1)\varepsilon}^{j\varepsilon} A_\varepsilon u_\varepsilon'\,dx \Big) dx \\
&\quad + \varepsilon^{-2} \int_{(j-1)\varepsilon}^{j\varepsilon} A_0 z'\,dx \int_{(j-1)\varepsilon}^{j\varepsilon} \frac{A_0 - A_\varepsilon}{A_0 A_\varepsilon}\,dx \int_{(j-1)\varepsilon}^{j\varepsilon} A_\varepsilon u_\varepsilon'\,dx \Bigg).
\end{aligned}$$

We have divided the integral into integrals over the periods of the coefficients and subtracted and added mean values of functions on these periods. This allows us, by several applications of the Cauchy-Schwarz and the Poincaré inequality (see Theorems A.22,A.24), to estimate the first two summands by multiples of ε,

$$\begin{aligned}
\|u_\varepsilon - u_0\|_{L^2(0,1)}^2 &\le \varepsilon \pi^{-1} \sum_{j=1}^N \Bigg(\Big\| \tfrac{A_0 - A_\varepsilon}{A_0 A_\varepsilon} \Big\|_{L^\infty((j-1)\varepsilon, j\varepsilon)} \|A_0 z''\|_{L^2((j-1)\varepsilon, j\varepsilon)} \|A_\varepsilon u_\varepsilon'\|_{L^2((j-1)\varepsilon, j\varepsilon)} \\
&\quad + \Big\| \tfrac{A_0 - A_\varepsilon}{A_0 A_\varepsilon} \Big\|_{L^\infty((j-1)\varepsilon, j\varepsilon)} \|A_0 z'\|_{L^2((j-1)\varepsilon, j\varepsilon)} \|(A_\varepsilon u_\varepsilon')'\|_{L^2((j-1)\varepsilon, j\varepsilon)} \Bigg) \\
&\quad + \varepsilon^{-2} \sum_{j=1}^N \Bigg(\int_{(j-1)\varepsilon}^{j\varepsilon} A_0 z'\,dx \int_{(j-1)\varepsilon}^{j\varepsilon} \frac{A_0 - A_\varepsilon}{A_0 A_\varepsilon}\,dx \int_{(j-1)\varepsilon}^{j\varepsilon} A_\varepsilon u_\varepsilon'\,dx \Bigg).
\end{aligned}$$

The third term on the right-hand side tends to zero (as $\varepsilon \to 0$) if and only if it is actually zero. This is achieved by the unique choice

$$A_0 := \left(\varepsilon^{-1} \int_{(j-1)\varepsilon}^{j\varepsilon} A_\varepsilon^{-1}\, dx\right)^{-1} = \left(\int_0^1 A_1^{-1}\, dx\right)^{-1} = \left(\int_0^1 A_\varepsilon^{-1}\, dx\right)^{-1}.$$

The discrete Cauchy-Schwarz inequality, hence, yields the error estimate

$$\begin{aligned}\|u_\varepsilon - u_0\|_{L^2(0,1)}^2 \le \varepsilon\pi^{-1}\Big(&\Big\|\tfrac{A_0 - A_\varepsilon}{A_0 A_\varepsilon}\Big\|_{L^\infty((j-1)\varepsilon, j\varepsilon)} \|A_0 z''\|_{L^2(0,1)} \|A_\varepsilon u_\varepsilon'\|_{L^2(0,1)} \\ &+ \Big\|\tfrac{A_0 - A_\varepsilon}{A_0 A_\varepsilon}\Big\|_{L^\infty((j-1)\varepsilon, j\varepsilon)} \|A_0 z'\|_{L^2(0,1)} \|(A_\varepsilon u_\varepsilon')'\|_{L^2(0,1)}\Big).\end{aligned}$$

Since

$$\begin{aligned} -A_0 z'' &= u_\varepsilon - u_0 \quad \text{in the sense of } L^2(0,1), \\ \|A_0 z'\|_{L^2(0,1)} &\le \pi^{-1} \|u_\varepsilon - u_0\|_{L^2(0,1)}, \\ -(A_\varepsilon u_\varepsilon')' &= f \quad \text{in the sense of } L^2(0,1), \text{ and} \\ \|A_\varepsilon u_\varepsilon'\|_{L^2(0,1)} &\le \pi^{-1} \sqrt{\beta/\alpha} \|f\|_{L^2(0,1)}, \end{aligned}$$

with $\alpha := \inf_{0<x<1} A_1(x) > 0$ and $\beta := \sup_{0<x<1} A_1(x) \ge \alpha$, we finally get

$$\|u_\varepsilon - u_0\|_{L^2(0,1)} \le \varepsilon \tfrac{2}{\alpha\pi^2} \left(1 + \sqrt{\beta/\alpha}\right) \|f\|_{L^2(0,1)}.$$

The previous calculations show that the desired effective coefficient A_0 exists, and moreover that the corresponding macroscopic solution approximates the true solution u_ε with an accuracy proportional to ε in $L^2(0,1)$. Note that the effective coefficient is the harmonic mean of A_ε rather than the simple average. As A_0 is easily computed by (numerical) quadrature to high accuracy in this simple model problem, we also have access to reliable and accurate numerical approximation of u_0 by standard schemes such as the P1-FEM introduced in the previous section. Since the coefficient is a global constant, the Aubin-Nitsche duality trick, Céa's lemma and standard interpolation error estimates show that for any $f \in L^2(0,1)$ the Galerkin finite element approximation $u_{0,H} \in V_H$ of u_0 computed on a uniform mesh $\mathcal{T}_H$ of width $H > 0$ satisfies

$$\|u_0 - u_{0,H}\|_{L^2(0,1)} \le \tfrac{1}{A_0\pi^2} H^2 \|f\|_{L^2(0,1)}.$$

Hence, for a given fixed value of ε, a finite element computation on the discretization scale $H = \sqrt{\varepsilon}$ would yield an approximation of the macroscopic part of u_ε on the same order of accuracy as u_0 itself. In practical applications, it may still be too expensive to compute on the scale $\sqrt{\varepsilon}$. In this case, the numerical discretization parameter H should be chosen according to the available computational resources, accepting that the simulation commits some larger but still acceptable error. The

subsequent Matlab code generates the corresponding FE approximations $u_{0,H}$, given the data of Section 1.3.1.

Example 1.2 (Finite element approximation of homogenized problem (1.15)*).*

```
% script file for illustration of FEM for 1d oscillatory diffusion
clear all
close all

% define Interval
I = [0,1];

% define diffusivity
Aepsilon = @(x,epsilon) 1./(2+cos(2*pi*x./epsilon));
Aharmean = .5;

% forcing term
f = @(x) ones(size(x));

% solution
uepsilon = @(x,epsilon) x - x.^2 ...
              + epsilon*(-1/(2*pi)*x.*sin(2*pi*x/epsilon)...
                        + 1/(4*pi)*sin(2*pi*x/epsilon)...
                        - epsilon/(4*pi^2)*cos(2*pi*x/epsilon)+...
                        + epsilon/(4*pi^2));

u0 = @(x,epsilon) x - x.^2;

% finite element approximation on equi-distant grid
% loop over frequency
for k=1:8
    % define frequency
    epsilon = 2^(-2*k);
    A = @(x) Aepsilon(x,epsilon);
    u = @(x) uepsilon(x,epsilon);

    % finte element grid
    N = 1+2^(k); % number of grid points
    H(k) = 1/(N-1); % mesh size
    x = (0:H(k):1)';

    % stiffness matrix
    Ndof = N-2;
    S = Aharmean./H(k).*(sparse(1:Ndof,1:Ndof,2,Ndof,Ndof)...
                        + sparse(2:Ndof,1:Ndof-1,-1,Ndof,Ndof)...
                        + sparse(1:Ndof-1,2:Ndof,-1,Ndof,Ndof));

    % right hand side (approximated by nodal interpolation)
    rhs = H(k)*f(x(2:N-1));

    % solve
    uk = [0;S\rhs;0]; % extend to boundary

```

```
    % approximate errors by accurate numerical quadrature
    err(k) = 0; % error with respect to u
    err0(k) = 0; % error with respect to u0
    for j=1:N-1
        err(k) = err(k) + ...
                  quadgk(@(s) (u(s)-uk(j)...
                  - (uk(j+1)-uk(j))./H(k)*(s-x(j))).^2,...
                    x(j),x(j+1),'RelTol',1e-8);
        err0(k) = err0(k) + ...
                   quadgk(@(s) (u0(s)-uk(j)...
                       - (uk(j+1)-uk(j))./H(k)*(s-x(j))).^2,...
                          x(j),x(j+1),'RelTol',1e-8);
    end
    err(k) = sqrt(err(k));
    err0(k) = sqrt(err0(k));
end

% plot errors
loglog(2.^(-2:-2:-16),err,'-bd','LineWidth',2);
hold on
loglog(2.^(-2:-2:-16),err0,'-mx','LineWidth',2);
l = legend('$\|u_\varepsilon - u_{0,H}\|_{L^2(0,1)}$',...
          '$\|u_0 - u_{0,H}\|_{L^2(0,1)}$','Location','NorthWest');
set(l,'Interpreter','latex')
set(gca,'Fontsize',18,'xscale','log','yscale','log',...
    'xtick',10.^(-5:1:1),'ytick',10.^(-7:1:-1))
axis([1e-5 1 1e-7 1e-1]);
axis square
grid on
xlabel('$\varepsilon$','Fontsize',18,'Interpreter','latex')
ylabel('$L^2 error$','Fontsize',18,'Interpreter','latex')

latexprint('../../LectureNotes/gfx/oscdiff1d_femhomerr','-r600')
```

The errors $(u_0 - u_{0,H})$ and $(u_\varepsilon - u_{0,H})$ are depicted in Figure 1.4 for several values of ε and two choices of coupling between H and ε to confirm the previous discussion of the theoretical results.

1.3.3 Numerical homogenization of general L^∞ coefficients

As we shall see later in this lecture, periodic homogenization may be generalized to higher space dimensions [4]. Even more general coefficients can be treated in the framework of G- or H-convergence [14, 17, 6]. However, in those cases, the characterization of the effective coefficient is usually not explicit anymore and requires numerical methods for its evaluation, e.g., the Heterogeneous Multiscale Method (HMM) [7, 8, 1]. Moreover, homogenization in the classical analytical sense considers a sequence of operators $-\operatorname{div}(A_\varepsilon \nabla \cdot)$ and aims to characterize the limit as ε

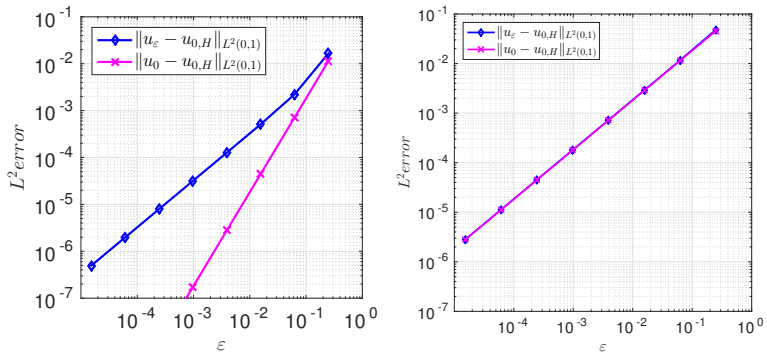

(a) $H = \varepsilon$. (b) $H = \sqrt{\varepsilon}$.

Fig. 1.4 Finite element approximation of homogenized model problem (1.15): L^2-error vs. diffusion parameter ε for two choices of the mesh size $H = \varepsilon$ (a) and $H = \sqrt{\varepsilon}$ (b).

tends to zero. In many realistic applications, e.g. in geophysics, (cf. Figure 1.5), such a sequence of models can hardly be identified or may not be available at all.

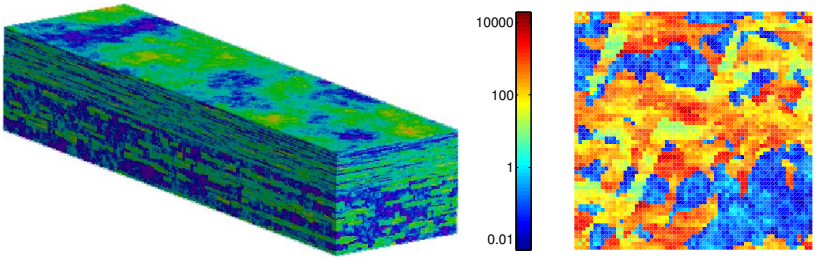

(a) 3d data. (b) 2d slice with scale.

Fig. 1.5 Strongly heterogeneous data from SPE10 benchmark; see `www.spe.org/web/csp/`.

That is why we are interested in the computation of effective representations of very rough unstructured coefficients. In the context of our model problem and the concept of a weak solution, $L^\infty(0,1)$ is the most general space of possible coefficients with the additional requirement of uniform positivity. For this section, we assume that $A \in L^\infty(0,1)$ and that there exists constants α,β such that

$$0 < \alpha \leq \inf_{0<x<1} A(x) \leq \sup_{0<x<1} A(x) \leq \beta < \infty. \tag{1.16}$$

The set of admissible coefficients will be denoted

$$\mathcal{M}([0,1],\alpha,\beta) := \{A \in L^\infty(0,1) \,|\, A \text{ satisfies (1.16)}\}. \tag{1.17}$$

Note that A is fairly free to vary within the bounds α and β and that we do not assume any frequencies of variation or smoothness.

Consider the model problem (1.8) with A_ε replaced with such a general $A \in \mathcal{M}([0,1],\alpha,\beta)$ and some forcing term $f \in L^2(0,1)$. The problem admits a unique solution u in the Sobolev space $H^1_0(0,1)$ that is as well characterized by the variational formulation

$$\int_0^1 Au'v'\,dx = \int_0^1 fv\,dx \quad \text{for all } v \in H^1_0(0,1). \tag{1.18}$$

The aim of this section is to revisit the derivation of the previous section to see if the assumption of periodicity was really essential. We consider a general grid of $N+2$ points

$$0 := x_0 < x_1 < x_2 < \ldots < x_{N+1} =: 1.$$

We shall introduce the corresponding finite element mesh

$$\mathcal{T}_H := \{T = [x_j, x_{j+1}] \,|\, j = 0,1,\ldots,N\}.$$

Although the mesh may be fairly general in terms of its local mesh size, we shall refer only to the global mesh size parameter $H := \max_{T\in\mathcal{T}_H} |T|$. The discretization parameter H is related to the target scale of interest or observation and we are interested to compute an effective coefficient that represents the solution of the model problem on all scales larger or equal to the local mesh size. More precisely, we are looking for an admissible coefficient A_H that is piecewise constant with respect to the mesh $\mathcal{T}_H$, i.e.,

$$A_H \in \mathcal{M}(\mathcal{T}_H,\alpha,\beta) := \{B \in \mathcal{M}([0,1],\alpha,\beta) \mid \forall T \in \mathcal{T}_H : B|_T \text{ is constant}\}. \tag{1.19}$$

We will follow closely the derivation of the previous subsection. Revisiting the arguments shows that periodicity was used to argue that A_0 is a global constant whereas the other arguments carry over to the present setting. Hence, the following lines do not carry any new mathematical arguments. However, as notation has changed a bit, we recall everything in detail.

For the time being, we assume that $A_H \in \mathcal{M}(\mathcal{T}_H,\alpha,\beta)$ and that the tentative macroscopic part u_H solves

$$\int_0^1 A_H u_H' v'\,dx = \int_0^1 f v_H\,dx \quad \text{for all } v \in H^1_0(0,1). \tag{1.20}$$

We shall have a look at the L^2-error between u and u_H. Since the error $(u-u_H) \in H^1_0(0,1) \subset L^2(0,1)$, there exists a unique $z \in H^1_0(0,1)$ such that

$$\int_0^1 A_H z' w'\,dx = \int_0^1 (u-u_H) w\,dx \quad \text{for all } w \in H^1_0(0,1).$$

The choice $w = (u-u_H)$ as a test function yields that

$$\|u-u_H\|^2_{L^2(0,1)} = \int_0^1 A_H z'(u-u_H)'\,dx.$$

The solutions u and u_H are linked by the equality of fluxes

$$Au' = A_H u_H' \qquad \text{in } H^{-1}(0,1).$$

The same arguments as in the previous Section lead to

$$\begin{aligned}\|u-u_H\|^2_{L^2(0,1)} \le \pi^{-1} \sum_{T\in\mathcal{T}_H} |T|\Big(&\Big\|\tfrac{A_H-A}{A_HA}\Big\|_{L^\infty(T)}\|(A_Hz')'\|_{L^2(T)}\|Au'\|_{L^2(T)}\\ &+\Big\|\tfrac{A_H-A}{A_HA}\Big\|_{L^\infty(T)}\|A_Hz'\|_{L^2(T)}\|(Au')'\|_{L^2(T)}\Big)\\ &+\sum_{j=1}^N |T|^{-2}\Big(\int_T A_Hz'\,dx\int_T\frac{A_H-A}{A_HA}\,dx\int_T Au'\,dx\Big).\end{aligned}$$

The third term on the right-hand side is eliminated by the unique choice

$$A_H|_T := \left(|T|^{-1}\int_T A^{-1}\,dx\right)^{-1} \text{ for any } T\in\mathcal{T}_H. \tag{1.21}$$

The discrete Cauchy-Schwarz inequality, hence, yields the error estimate

$$\begin{aligned}\|u-u_H\|^2_{L^2(0,1)} \le H\pi^{-1}\Big(&\Big\|\tfrac{A_H-A}{A_HA}\Big\|_{L^\infty(0,1)}\|(A_Hz')'\|_{L^2(0,1)}\|Au'\|_{L^2(0,1)}+\\ &\Big\|\tfrac{A_H-A}{A_HA}\Big\|_{L^\infty(0,1)}\|A_Hz'\|_{L^2(0,1)}\|(Au')'\|_{L^2(0,1)}\Big).\end{aligned}$$

Since

$$\begin{aligned}-(A_Hz')' &= u-u_H \quad \text{in the sense of } L^2(0,1),\\ \|A_Hz'\|_{L^2(0,1)} &\le \pi^{-1}\sqrt{\beta/\alpha}\|u-u_H\|_{L^2(0,1)},\\ -(Au')' &= f \quad \text{in the sense of } L^2(0,1), \text{ and}\\ \|Au'\|_{L^2(0,1)} &\le \pi^{-1}\sqrt{\beta/\alpha}\|f\|_{L^2(0,1)},\end{aligned}$$

we finally get

$$\|u-u_H\|_{L^2(0,1)} \le H\frac{4}{\alpha\pi^2}\sqrt{\beta/\alpha}\|f\|_{L^2(0,1)}. \tag{1.22}$$

Homogenization in the classical sense is, hence, achieved whenever one is able to find a mesh $\mathcal{T}_H$ such that the numbers $A_H|_T$ coincide for all $T\in\mathcal{T}_H$. In the periodic case, this happens for any equidistant mesh that is in resonance with the frequency of the coefficient (i.e., H is an integer multiple of ε). In the general case A_H is only $\mathcal{T}_H$-piecewise constant.

Note that u_H may now be replaced with its Galerkin projection onto the P1-FE space on the same mesh $\mathcal{T}_H$ without any harm. Similar as in the previous subsection, we may also consider its Galerkin approximation on an even coarser mesh of width $\sqrt{H}$. However, on this scale, A_H is not a constant in each element and such an approach may suffer from possible oscillations of A_H on the scale H.

1.3.4 A different approach to numerical homogenization

Another approach to numerical homogenization of (1.18) (or (1.6) in general) is that of the approximation of the solution space $H_0^1(0,1)$ by a finite-dimensional space as in Subsection 1.3.1 but without undesired scale-dependent pre-asymptotic effects. In what follows, we shall illustrate that this is possible.

Given positive constants $\beta \geq \alpha > 0$, some admissible coefficient $A \in \mathcal{M}([0,1],\alpha,\beta)$ and some forcing term $f \in L^2(0,1)$, we wish to approximate the unique function $u \in H_0^1(D)$ that satisfies the variational problem (1.18)

$$\int_0^1 Au'v'\,dx = \int_0^1 fv\,dx \quad \text{for all } v \in H_0^1(0,1). \tag{1.23}$$

While in the two previous subsections the aim was to approximate A by some effective coefficient A_H and a corresponding effective problem that is easily solved by means of standard finite elements, we are now heading for a generalized finite element method that encodes the unresolvable fine-scale information in its shape functions. This is a fully discrete approach in the sense that the effective problem will be a discrete one.

As in Subsection 1.3.3, we consider a fairly general mesh $\mathcal{T}_H := \{T = [x_j, x_{j+1}] \,|\, j = 0,1,\ldots,N\}$ represented by $N+2$ grid points

$$0 := x_0 < x_1 < x_2 < \ldots < x_{N+1} =: 1.$$

The global mesh size parameter is $H := \max_{T\in\mathcal{T}_H} |T|$ and we use a capital letter to emphasize that H may be arbitrarily coarse and possibly larger than characteristic length scales of the coefficient A, if any.

Our goal is to design a finite-dimensional space $\tilde{V}_H \subset V := H_0^1(0,1)$ (linked to the mesh $\mathcal{T}_H$) with a local basis and high-approximation properties regardless of variations of A. In particular we want the space to be accurate in the pre-asymptotic regime of the standard FEM observed in Subsection 1.3.1. Our starting point will be the standard finite element space

$$V_H = \{v_H \in H_0^1(0,1) \,|\, \forall T \in \mathcal{T}_H : v_H|_T \in \mathbb{P}_1\} \tag{1.24}$$

of continuous $\mathcal{T}_H$-piecewise affine functions that vanish at the boundary of the unit interval previously defined in (1.12). We shall also characterize the functions of the solution space $V = H_0^1(0,1)$ that are not well captured by V_H. Define

$$W_H := \{w \in H_0^1(0,1) \,|\, \forall\, j = 1,\dots,N_H : w(x_j) = 0\}. \tag{1.25}$$

We will refer to this space as the fine scale or microscopic space. Its elements oscillate at frequencies larger than H^{-1}. Observe that any function $v \in V$ can be cast in the form $v_H \in V_H$ plus $w_H \in W_H$, where v_H is the nodal interpolation of v at the vertices x_j and w_H is the error of interpolation. Recall that point evaluation is well posed for univariate H_0^1 functions in the sense of the Sobolev embedding $H^1(0,1) \hookrightarrow C([0,1])$ (cf. Theorem A.19). In other words,

$$V = V_H \oplus W_H.$$

This decomposition is orthogonal in $H_0^1(0,1)$, i.e., for any $v_H \in V_H$ and any $w_H \in W_H$ it holds

$$\int_0^1 v_H'(x) w_H'(x)\,dx = \sum_{T \in \mathcal{T}_H} (v_H|_T)' \int_T w_H'(x)\,dx = 0.$$

However, the experiment of Subsection (1.3.1) clearly indicates that this orthogonality has no impact in the context of the model problem (1.18) which is related to a different scalar product.

Instead, the new approach to numerical homogenization of this section is based on the orthogonalization of this decomposition with respect to the scalar product

$$a(\cdot,\cdot) := \int_0^1 A(\cdot)'(\cdot)'\,dx$$

induced by the model problem (1.18). Keeping the characterization of fine scales W_H fixed, this orthogonalization characterizes a new coarse space $\tilde{V}_H$ by

$$V = \tilde{V}_H \oplus W_H \quad \text{and} \quad \tilde{V}_H \perp_a W_H.$$

A Galerkin method based on $\tilde{V}_H$ computes the a-orthogonal projection $\tilde{u}_H \in \tilde{V}_H$ of the unknown solution $u \in V$ onto $\tilde{V}_H$, i.e., $\tilde{u}_H$ is the unique function in $\tilde{V}_H$ that satisfies

$$a(\tilde{u}_H, \tilde{v}_H) = \int_0^1 f(x)\tilde{v}_H(x)\,dx \;\text{ for all } \tilde{v}_H \in \tilde{V}_H. \tag{1.26}$$

By Galerkin orthogonality,

$$a(u - \tilde{u}_H, \tilde{v}_H) = 0 \;\text{ for all } \tilde{v}_H \in \tilde{V}_H,$$

the error $(u - \tilde{u}_H) \in W_H$ is a fine scale function. Hence, the error of this method vanishes in all mesh points, i.e., $\tilde{u}_H$ interpolates u in the grid points x_j ($j = 0,\dots,N+1$). This, Friedrichs' inequality (cf. Theorems A.23,A.24), Galerkin orthogonality, symmetry of the bilinear form a and the Cauchy-Schwarz inequality yield

$$\begin{aligned}\|u-\tilde{u}_H\|^2_{L^2(0,1)} &\le \frac{H^2}{\pi^2}\|(u-\tilde{u}_H)'\|^2_{L^2(0,1)}\\ &\le \alpha^{-1}\frac{H^2}{\pi^2}\int_0^1 A(u-\tilde{u}_H)'(u-\tilde{u}_H)'\,dx\\ &= \alpha^{-1}\frac{H^2}{\pi^2}\int_0^1 Au'(u-\tilde{u}_H)'\,dx\\ &= \alpha^{-1}\frac{H^2}{\pi^2}\int_0^1 f(u-\tilde{u}_H)dx\\ &\le \alpha^{-1}\frac{H^2}{\pi^2}\|f\|_{L^2(0,1)}\|u-\tilde{u}_H\|_{L^2(0,1)},\end{aligned}$$

and, hence, the error estimate

$$\|u-\tilde{u}_H\|_{L^2(0,1)} \le \alpha^{-1}\frac{H^2}{\pi^2}\|f\|_{L^2(0,1)}. \tag{1.27}$$

This means that the error of the method is proportional to the discretization parameter H squared, unconditionally for all H and independent of the coefficient A. In contrast to the homogenized solution and the standard finite element approximation, the approximation $\tilde{u}_H$ encodes also fine scale information. A truly coarse approximation would be the finite element part of $\tilde{u}_H$, that is, its nodal interpolation $I_H\tilde{u}_H \in V_H$ defined by $I_H\tilde{u}_H(x_j) = \tilde{u}_H(x_j)(= u(x_j))$ for all $j = 0, 1, \ldots, N_H$. Note that $I_H\tilde{u}_H$ still enjoys the favorable error estimate

$$\|u-I_H\tilde{u}_H\|_{L^2(0,1)} \le \alpha^{-1/2}\frac{H}{\pi}\|f\|_{L^2(0,1)}. \tag{1.28}$$

Another remark concerns the treatment of the right-hand side. Note that the new approach affects not only the discrete differential operator but also the right-hand side because the test functions are modified. Replacing the right-hand side $\tilde{v}_H \mapsto \int_0^1 f\tilde{v}_H\,dx$ in (1.26) with $\tilde{v}_H \mapsto \int_0^1 fI_H(\tilde{v}_H)\,dx$ removes this problem and leads to a modified method

$$a(\tilde{u}_H, \tilde{v}_H) = \int_0^1 f(x)I_H\tilde{v}_H(x)\,dx \quad \text{for all } \tilde{v}_H \in \tilde{V}_H. \tag{1.29}$$

Note that the solutions of (1.26) and (1.29) do not coincide but their H^1 distance can be controlled by the term $H\|f\|_{L^2(0,1)}$ so that the error bounds (1.27) and (1.28) remain valid in terms of the rate of convergence H^2 and H, respectively.

It remains to find a local basis of the space $\tilde{V}_H$ so that the discretization leads to a sparse linear system that can be solved efficiently. Starting from the nodal basis

$$\{\Lambda_j \in V_H \,|\, \Lambda_j(x_i) = \delta_{ij} \text{ for } i, j = 1, 2, \ldots, N_H - 1\}$$

of V_H, the Schmidt-type orthogonalization yields that

$$\tilde{V}_H = \operatorname{span}\{\tilde{\Lambda}_j := \Lambda_j - \phi_j \,|\, j = 1, 2, \ldots, N_H - 1\},$$

where the correction $\phi_j \in W_H$ is such that

$$a(\phi_j, w) = a(\Lambda_j, w) \quad \text{for all } w \in W_H. \tag{1.30}$$

Since the right hand side vanishes for test functions $w \in W_H$ which do not have support in the elements T_j, T_{j+1} adjacent to x_j, (1.30) is equivalent to solve the local problems

$$a(\phi_j|_{T_j}, w) = H^{-1} \int_{T_j} Aw' \, dx \quad \text{for all } w \in H_0^1(T_j), \tag{1.31}$$

$$a(\phi_j|_{T_{j+1}}, w) = -H^{-1} \int_{T_{j+1}} Aw' \, dx \quad \text{for all } w \in H_0^1(T_{j+1}). \tag{1.32}$$

This implies that $\operatorname{supp}\tilde{\Lambda}_j \subset \operatorname{supp}\Lambda_j$ for all j. Moreover, since $\phi|_{T_{j+1}} = -\phi|_{T_j}$, the ϕ_j can be computed by solving (1.31) for all $T \in \mathcal{T}_H$. The local problems (1.31) are denoted corrector problems. For periodic coefficients and if the mesh size H is an integer multiple of the period (!), only one of these problems for an arbitrary element $T \in \mathcal{T}_H$ needs to be solved. In the one-dimensional case the corrector problems are easily solved analytically by hand. It turns out that for any $j = 1, 2, \ldots, N_H$,

$$\tilde{\Lambda}_j(x) := \begin{cases} \dfrac{\int_{x_{j-1}}^{x} A^{-1}(s)\,ds}{\int_{x_{j-1}}^{x_j} A^{-1}(s)\,ds}, & \text{if } x \in T_j, \\ 1 - \dfrac{\int_{x_j}^{x} A^{-1}(s)\,ds}{\int_{x_j}^{x_{j+1}} A^{-1}(s)\,ds}, & \text{if } x \in T_{j+1}, \\ 0, \quad \text{else.} \end{cases} \tag{1.33}$$

See Figure 1.6 for a visualization of this perturbed nodal basis given the oscillatory coefficient from (1.10) with $\varepsilon = 2^{-5}$. In the literature, this method and its variants are known under several names, e.g., Generalized FEM (GFEM) [3], Variational Multiscale Method [12], Multiscale FEM (MsFEM) [11] or Residual Free Bubbles [5]. The previous derivation is based on the interpretation of [13]; see also [10, 15].

We shall have a closer look at the relation of the current approach with the method of the previous Section 1.3.3. Recall that the nodal values $\tilde{u}_H(x_j)$ of the Galerkin approximation $\tilde{u}_H = \sum_{j=1}^{N} \tilde{u}_H(x_j)\tilde{\Lambda}_j$ are the unique solution of the system of N linear equations

$$\sum_{k=1}^{N} \left(\int_0^1 A\tilde{\Lambda}_j' \tilde{\Lambda}_k' \, dx \right) \tilde{u}(x_k) = \int_0^1 f\Lambda_j \, dx, \quad j = 1, \ldots, N.$$

Using the explicit representation of $\tilde{\Lambda}_j$, this system is easily rewritten as

$$\sum_{k=1}^{N} \left(\int_0^1 A_H \Lambda_j' \Lambda_k' \, dx \right) \tilde{u}(x_k) = \int_0^1 f\Lambda_j \, dx, \quad j = 1, \ldots, N,$$

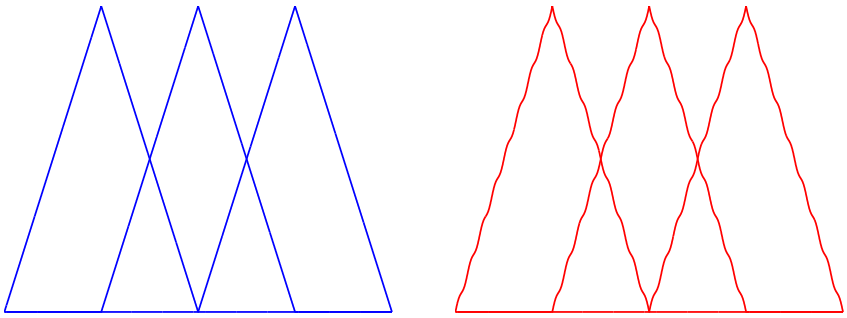

(a) Classical nodal basis. (b) Perturbed nodal basis.

Fig. 1.6 Classical nodal basis on uniform mesh $\mathcal{T}_H$ ($H = .25$) and corrected nodal basis for numerical homogenization (coefficient A_ε as in (1.10) with $\varepsilon = 2^{-5}$).

where A_H is exactly the homogenized coefficient defined in (1.21). This means that the method of this section is equivalent to computing the homogenized coefficient with respect to $\mathcal{T}_H$ as in the previous section followed by a P1-FE approximation of the corresponding homogenized solution characterized by (1.20) on the same mesh $\mathcal{T}_H$.

The previous derivations indicate the possible superiority of numerical homogenization over analytical techniques with regard to its applicability beyond structural assumption on the coefficient. However, we shall warn the reader that all previous derivations -- related to numerical and analytical homogenization -- hold only in one space dimension. We have used, e.g. , that any $L^2(0,1)$ function is a gradient or that point evaluation for H^1 functions is a well-defined and stable operation. The main goal of this lecture will be to generalize the previous approaches to two- and three-dimensional settings. In this connection, the re-interpretation of numerical homogenization of this section will be of great value as it allows such a generalization even for L^∞ coefficients.

References

1. A. Abdulle. The finite element heterogeneous multiscale method: a computational strategy for multiscale PDEs. In *Multiple scales problems in biomathematics, mechanics, physics and numerics*, volume 31 of *GAKUTO Internat. Ser. Math. Sci. Appl.*, pages 133--181. Gakkōtosho, Tokyo, 2009.
2. Jean-Pierre Aubin. *Analyse fonctionnelle appliquée. Tome 1 & 2*. Mathématiques. [Mathematics]. Presses Universitaires de France, Paris, 1987.
3. I. Babuška and J. E. Osborn. Generalized finite element methods: their performance and their relation to mixed methods. *SIAM J. Numer. Anal.*, 20(3):510--536, 1983.
4. A. Bensoussan, J.-L. Lions, and G. Papanicolaou. *Asymptotic Analysis for Periodic Structures*. North-Holland Publ., 1978.

5. Franco Brezzi and Alessandro Russo. Choosing bubbles for advection-diffusion problems. *Math. Models Methods Appl. Sci.*, 4(4):571--587, 1994.
6. Ennio De Giorgi. Sulla convergenza di alcune successioni d'integrali del tipo dell'area. *Rend. Mat. (6)*, 8:277--294, 1975. Collection of articles dedicated to Mauro Picone on the occasion of his ninetieth birthday.
7. W. E and B. Engquist. The heterogeneous multiscale methods. *Commun. Math. Sci.*, 1(1):87--132, 2003.
8. W. E and B. Engquist. The heterogeneous multi-scale method for homogenization problems. In *Multiscale methods in science and engineering*, volume 44 of *Lect. Notes Comput. Sci. Eng.*, pages 89--110. Springer, Berlin, 2005.
9. Y. R. Efendiev and T. Y. Hou. *Multiscale finite element methods*, volume 4 of *Surveys and Tutorials in the Applied Mathematical Sciences*. Springer, New York, 2009. Theory and applications.
10. P. Henning and D. Peterseim. Oversampling for the multiscale finite element method. *Multiscale Modeling & Simulation*, 11(4):1149--1175, 2013.
11. Thomas Y. Hou and Xiao-Hui Wu. A multiscale finite element method for elliptic problems in composite materials and porous media. *J. Comput. Phys.*, 134(1):169--189, 1997.
12. T. J. R. Hughes. Multiscale phenomena: Green's functions, the Dirichlet-to-Neumann formulation, subgrid scale models, bubbles and the origins of stabilized methods. *Comput. Methods Appl. Mech. Engrg.*, 127(1-4):387--401, 1995.
13. A. Målqvist and D. Peterseim. Localization of Elliptic Multiscale Problems. *Mathematics of Computation (in press), also ArXiv e-prints*, 1110.0692, 2011.
14. F. Murat and L. Tartar. H-convergence. *Séminaire d'Analyse Fonctionnelle et Numérique de l'Université d'Alger*, 1978.
15. Daniel Peterseim. Variational multiscale stabilization and the exponential decay of fine-scale correctors. In G.R. Barrenechea, F. Brezzi, A. Cangiani, and E.H. Georgoulis, editors, *Building Bridges: Connections and Challenges in Modern Approaches to Numerical Partial Differential Equations*, volume 114 of *Lecture Notes in Computational Science and Engineering*, pages 343--369. Springer International Publishing, 2016.
16. L. A. Richards. Capillary conduction of liquids through porous mediums. *Journal of Applied Physics*, 1(5):318--333, 1931.
17. S. Spagnolo. Sulla convergenza di soluzioni di equazioni paraboliche ed ellittiche. *Ann. Scuola Norm. Sup. Pisa (3) 22 (1968), 571-597; errata, ibid. (3)*, 22:673, 1968.
18. H.W. Wilhelm and S. Luckhaus. Quasilinear elliptic-parabolic differential equations. *Mathematische Zeitschrift*, 183(3):311--341, 1983.